VOL. 17, NO. 6, JUNE 1979 AIAA JOURNAL 601
ARTICLE NO. 79-4080

Blast Waves Produced by a Time-Dependent Energy Source

Y. Oved,* F. Milinazzo,† R. M. Clements,‡
University of Victoria, Victoria, B.C., Canada
and
P. R. Smy§
University of Alberta, Edmonton, Alta., Canada

The dynamics of a spherical blast wave produced by an arbitrary time-dependent energy source are investigated both theoretically and experimentally. The blast wave in air is produced by an electrical discharge in a small cavity (a plasma jet used for internal combustion engine ignition). High-speed streak and Schlieren frame photography are used to measure the front of the self-luminous plasma and the shock wave, respectively. A numerical Eulerian model based on the gasdynamic equations in conservation form is used to predict positions of the luminosity front and the shock wave. Good agreement is obtained between theory and experiment.

I. Introduction

WE consider the situation in which energy is dissipated within a given volume of gas as a function of time; i.e., $E=f(r,t)$, where r is the space coordinate, t is time, and E is energy. As the gas is heated, its pressure increases and it expands into the surrounding cold gas. As energy continues to be dissipated, further heating of the rarefied gas near the origin occurs, forming a highly ionized plasma. A train of pressure waves propagates outward, with the waves that are emitted later in time propagating faster than the earlier ones (because they propagate into a hotter gas). As the latter waves overtake the earlier waves, a shock wave forms in front of the plasma.

The analytical theory describing blast waves was originally proposed independently by Taylor[1] and Sedov.[2] Since that time there has been a great deal of literature on the subject. For example, Refs. 3 and 4 devote sections to the subject. The early treatments assume that the energy is supplied instantaneously at $t=0$ to an infinitesimally small region of gas at $r=0$, that the resultant shock is strong, and that the transport properties are unimportant. Freeman[5] analytically investigates in detail the situation where the energy $E\propto t^{\beta}$ ($\beta=$const). Although he considers, in general, planar, cylindrical, and spherical blast waves, the majority of his detailed results are for cylindrically symmetric blast waves. Pitkin[6] extends Freeman's ideas and develops a computational algorithm which allows planar, cylindrical, and spherical geometries as well as noninteger values of β to be readily considered.

Freeman and Craggs[7] proceed to verify experimentally that the cylindrical blast wave produced during the early stages of spark-channel formation is indeed described by Freeman's theory in which $\beta=0$ (i.e., instantaneous energy release). Dabora[8] considers the experimental results of Hall,[9] in which a spherically symmetric blast wave is produced by focusing a Q-switched ruby laser onto a metallic target. He shows that Hall's results are best described by $\beta=0.1$ and not $\beta=0$. That is, even though the laser energy is released very rapidly ($\sim$20 ns), the resulting blast wave is best described by assuming that the energy input varies with time.

Numerical calculations of the flowfield behind a spherically symmetric blast wave for instantaneous energy input were first done by Brode.[10] The Taylor[1] solution was taken to be the initial value of the problem, and the numerical calculations were performed for the region in which the shock was weak. In this region no exact solution exists. Director and Dabora[11] considered energy $\propto t^{\beta}$ and obtained numerical solutions behind a spherical blast wave. Their experimental results[12] on spherical blast waves produced by a focused ruby laser for $\beta=0$ and $\beta=1$ showed reasonable agreement with the appropriate theory.[8,11]

In many situations of interest, the energy producing the blast wave cannot be considered to be dissipated either instantaneously or linearly with time. For example, the energy dissipated in a spark resulting from an ordinary capacitor discharge is often of rather long duration and has a complex waveform. One notes, for example, that Freeman and Craggs[7] use a somewhat unusual matched coaxial cable discharge circuit in order to supply energy to their spark fast enough that it can be considered instantaneous. Thus, if one wishes to understand the blast wave produced by a device of practical interest, it is frequently necessary to develop a model which will accommodate energy input of an arbitrary form. Such a numerical model has been developed by Milinazzo et al.[13] In the present paper, we use this model to investigate the propagation of a spherical blast wave and the luminous plasma behind it. The plasma is created by an electrical discharge in a small cavity which has one end open. This device is described in detail by Topham et al.[14] and is of practical interest as a high-energy igniter for internal combustion engines.[15-17]

The present study is limited to the early stages of the flow. During this time, the blast wave is approximately spherically symmetric. The position of the luminosity front, which is the front of the hot plasma, is measured with high-speed streak photography. The position of the shock front is measured with high-speed frame Schlieren photography. The measured electrical power dissipated in the discharge is supplied to the numerical model and the flow is computed. The computed luminosity and shock front positions are in good agreement with the measured results.

II. Experimental

A. Cavity and Power Input

The energy which produces the blast wave is generated by an electrical discharge in a small cylindrical cavity as shown schematically in Fig. 1. The electrical discharge circuit is the same as that described by Topham et al.[14] A high-voltage

Received Aug. 7, 1978; revision received Jan. 18, 1979.

Index category: Shock Waves and Detonations.

*Postdoctoral Fellow, Dept. of Physics.
†Visiting Assistant Professor, Dept. of Mathematics.
‡Associate Professor, Dept. of Physics.
§Assistant Dean of Engineering.

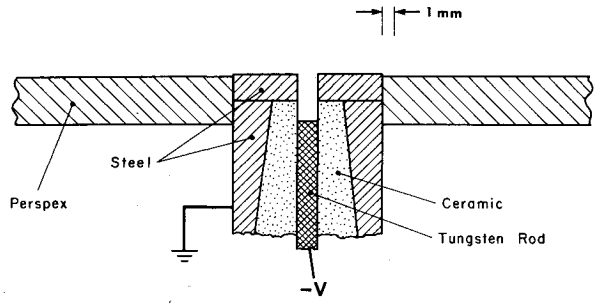

Fig. 1 Schematic of the discharge cavity geometry.

pulse applied to the plasma plug (Fig. 1) causes the initial breakdown between the center electrode and the end plate. The current required to sustain the arc is supplied by a 15 μF capacitor, which can be charged up to 900 V (i.e., a maximum stored energy of 6.1 J). This capacitor is coupled via an inductance to the center electrode of the cavity. The subsequent discharge has a ringing frequency of 9.3 kHz and all measurements are made in the air at STP. In order to determine the power being dissipated in the discharge, its current is measured with a standard inductively coupled current probe, while the voltage is a differential measurement between the center electrode and outer body of the cavity. Because of losses in the cable connecting the capacitor and the discharge cavity, only about one-half the stored energy is actually dissipated in the discharge.

B. Current Flow Outside the Cavity

In order to apply the numerical model of the blast wave to our experimental situation, it is necessary to know the spatial volume in which energy is dissipated. Specifically, is energy being dissipated throughout the whole volume of luminous plasma or merely within the discharge cavity? To answer this question, a thin wire (wire diameter $\approx 1/5$ cavity diameter) was positioned normal to the axis of symmetry of the cavity. The wire was connected to ground and the current through the wire measured as a function of distance between the wire and the cavity end plate. The presence of the wire did not appear to affect the plasma; it was found that as long as the plasma enveloped the wire, an appreciable amount of current flowed to the wire. The amount of current decreased from about 25% of the discharge current for distances of 1 mm to about 5% for distances of 1 cm. Although these measurements are not really quantitative (i.e., we cannot state the energy dissipated in a given spatial volume), they clearly indicate that energy is being dissipated in the plasma outside the cavity. Thus, they substantiate the assumption made in the numerical model that energy is being dissipated throughout the plasma volume.

C. Luminosity Front

Measurement of the position of the luminosity front was made using the smear camera described by Ramsay and Clements.[18] This is essentially a conventional rotating mirror-type camera with a maximum time resolution of 1 μs/mm. Its slit was along the axis of symmetry of the discharge cavity.

It was found experimentally that there is a delay in time between the initial flow of discharge current and the onset of emitted radiation. This delay measured with a photodiode is 3 μs. This value is the same as that found from the measurements described in the previous section when one extrapolates to zero distance between the wire and the cavity end plate.

D. Shock Wave

The position of the weak shock produced by the discharge is detected with high-speed Schlieren photography. The Schlieren system used is the one developed by Dewey and Walker,[19] in which frame photographs are obtained by using the light from a multiple pulse ruby laser.

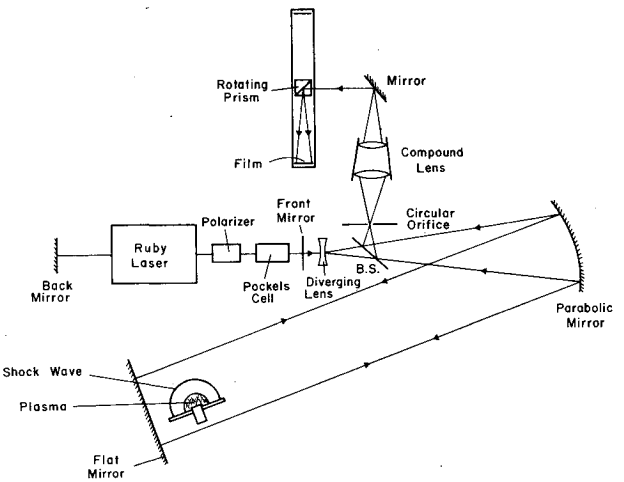

Fig. 2 Schematic of the double-pass Schlieren system.

The double-pass Schlieren system is shown in Fig. 2. The laser beam is expanded by the diverging lens and parabolic mirror. The expanded parallel beam is then passed through the flowfield under study, reflected back by the flat mirror through a beam-splitter, and then focused again. A circular orifice is used around the focal point of the beam and acts as a "knife edge." Then a rotating prism mounted inside a circular drum, finally sweeps the focused image over the film.

The width of the laser pulses is 20 ns, and the time between them can be reduced to about 20-30 μs. The output of the laser is monitored with a photodiode and this signal is superimposed on the measured discharge current.

Typical Schlieren photographs are shown in Fig. 3. We see that in the early stages, both the shock wave and the plasma near the origin have spherical symmetry. Later, the plasma jet develops and the shape of the plasma deviates from spherical symmetry. The surface irregularities may be Rayleigh-Taylor instabilities, in view of the fact that the light (hot) gas accelerates a dense (cold) gas.

III. Numerical Model

Because the volume of the cavity is very small in comparison with the volume of the flowfield under study, we assume that the flow has spherical symmetry. As our measurements indicate, this is a reasonable assumption for early times in the discharge history when the cylindrical plasma jet has not had time to develop.

The model assumes that the flow is described by the one-dimensional gasdynamics equations:

$$\frac{\partial \rho}{\partial t} + \frac{1}{r^2}\frac{\partial}{\partial r}(r^2 U\rho) = 0 \tag{1}$$

$$\frac{\partial}{\partial t}(\rho U) + \frac{1}{r^2}\frac{\partial}{\partial r}(r^2 U\rho U) + \frac{\partial P}{\partial r} = 0 \tag{2}$$

$$\frac{\partial \epsilon}{\partial t} + \frac{1}{r^2}\frac{\partial}{\partial r}(r^2 U\epsilon) + \frac{1}{r^2}\frac{\partial}{\partial r}(r^2 PU) = F(r,t) \tag{3}$$

The energy per unit volume ϵ, the mass density ρ, the gas velocity U, and the pressure P are related by the equation of state

$$\epsilon = P/(\gamma - 1) + \tfrac{1}{2}\rho U^2 \tag{4}$$

with γ, the ratio of the specific heats of the gas, equal to 1.4. These equations express the conservation of mass,

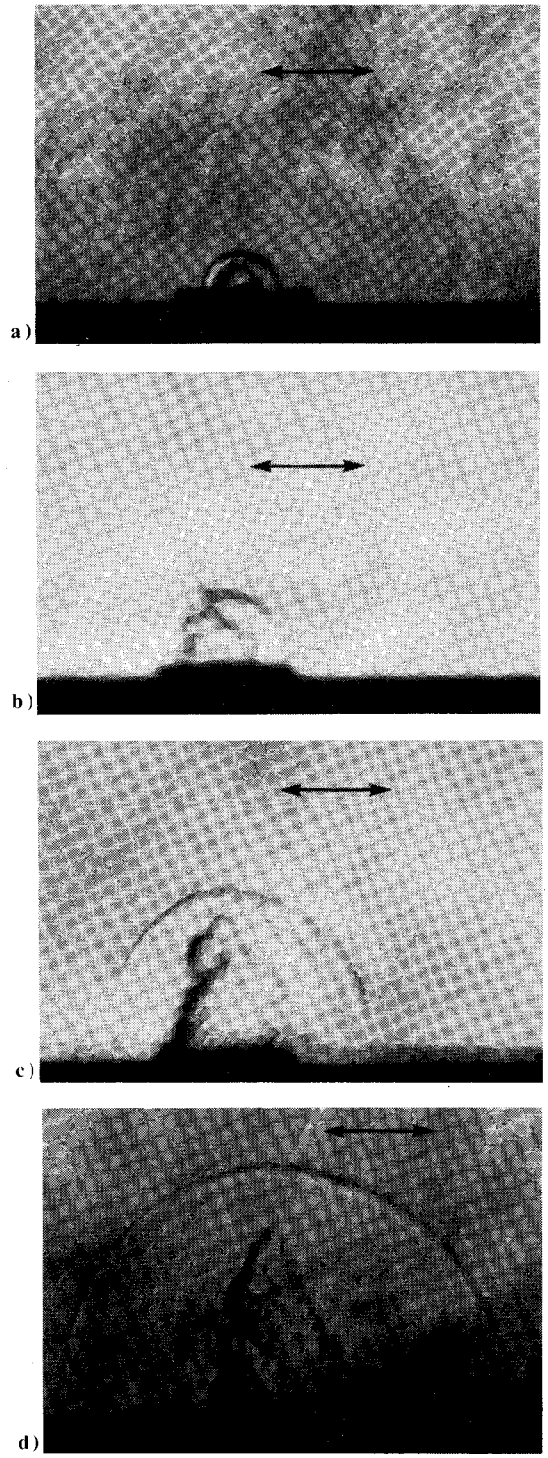

Fig. 3 Typical Schlieren photographs for 900 V. The times are: a) 9 μs, b) 16 μs, c) 29 μs, and d) 50 μs after the time power begins to be dissipated in the cavity. The arrow in each photograph is 1.0 cm long.

momentum, and energy where the effects[1-7,11] of radiation, heat conduction, and diffusion are negligible. Losses to the cavity and the walls are also neglected.

It is assumed that initially the gas is at rest with ρ, P equal to their ambient values, and $U=0$.

To Eqs. (1-4) we add the boundary conditions

$$\frac{\partial \rho}{\partial r}(o,t)=0 \qquad \frac{\partial \rho}{\partial r}(R_{\max},t)=0$$

$$U(o,t)=0 \qquad \frac{\partial U}{\partial r}(R_{\max},t)=0$$

$$\frac{\partial \epsilon}{\partial r}(o,t)=0 \qquad \frac{\partial \epsilon}{\partial r}(R_{\max},t)=0 \tag{5}$$

where $R_{\max}$ is the length of the region of interest. In all our computations, the position of the shock front is smaller than $R_{\max}$.

The numerical solution of Eqs. (1-4) in Eulerian form with the boundary conditions from Eq. (5) is based on the flux-corrected transport (FCT) algorithm[20-24] (a detailed description of which is given in Ref. 13). Our grid consists of N-concentric spherical shells (N was 100-200).

The FCT algorithm proceeds in two stages. The first stage computes the physical transport of mass between adjacent shells; this includes the convective transport of mass due to the source term in Eq. (3). The second stage introduces a diffusion term to avoid small-scale numerical oscillations near sharp gradients. An antidiffusion term is included to reduce the residual diffusion and to maintain the overall accuracy of the algorithm.

The program can handle any type of time-dependent energy source; the power input can be supplied as an analytic function of any type or taken from experimental data as was done in the present case.

If in the numerical model one assumes that the energy is dissipated in the same volume as that of the cavity, high temperatures and particle velocities are obtained. In fact, the program will not run for times beyond 3 μs. However, as discussed in an earlier section, there is strong experimental evidence to indicate that energy is dissipated throughout the volume behind the luminous plasma front. This of course implies that the volume in which energy is being dissipated is not constant but increases as a function of time. Thus, we assume that energy is dissipated uniformly in the hemispherical volume behind the luminosity front. The positions of the luminosity front and the shock front are calculated numerically, assuming them to be located at the largest negative gradient of the temperature distribution and the density distribution of the gas. Numerical calculations[13] reveal that the propagation of the luminosity front is more strongly affected than any other measurable quantity by the variation of the volume in which energy is dissipated. Thus, in this paper, the majority of our experimental measurements are of the position of the luminosity front.

In order to avoid computational problems at $t=0$ the initial volume in which energy is dissipated is chosen to be the volume of the cavity. This corresponds to a hemisphere of radius 0.8 mm. Thus, for comparison between the calculations and experiment, it was necessary to shift the calculated spatial coordinate by −0.8 mm. In addition, the delay in emitted radiation from the cavity (see Sec. II. C.) is accounted for by subtracting 3 μs from the time coordinate.

IV. Results and Discussion

We present our results in dimensional variables. In Refs. 3-8, 11, and 12, the form of the energy input is $E_\alpha = W_\alpha t^\beta$ and W_α determines both the time and length scales.[5] In our work, the form of the power input differs from case to case and does not provide us with a convenient energy scale. Thus, there are no scales which would allow us to present our results in a meaningful nondimensional form.

The results of the measured and calculated positions of the luminosity front are shown in Figs. 4a-e for voltages of 200, 300, 450, 600, and 900 V, respectively. These are the voltages to which the 15 μF energy storage capacitor is charged. The agreement between theory and experiment is good. One should also note that the shape of the measured power vs time curves are somewhat unusual. This is especially true for the lower voltages in which the potential across the discharge is only slightly more than the maintaining voltage of the discharge. Thus, there are abrupt changes in power. It is clear from Figs. 3c and 3d that the assumption of a spherically

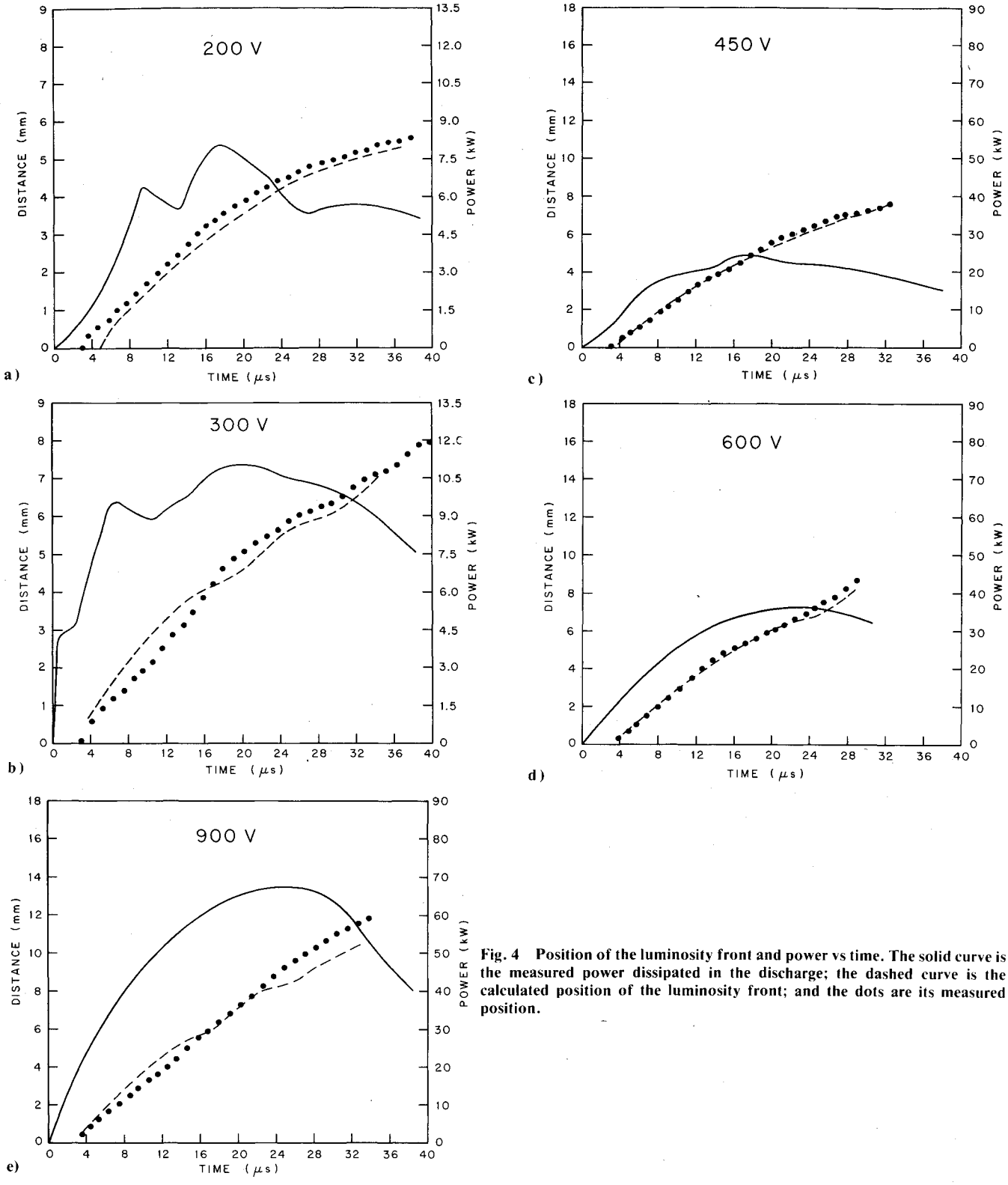

Fig. 4 Position of the luminosity front and power vs time. The solid curve is the measured power dissipated in the discharge; the dashed curve is the calculated position of the luminosity front; and the dots are its measured position.

symmetric luminous front is not applicable at later times. For these times the luminous front is more conical than spherical. Thus, the comparison between the measured and predicted positions of the luminous front are made only for small enough values of time so that the assumption of spherical symmetry is reasonable. More detailed consideration of the results shows that in the case of 200 V, the theory is below the experimental results. In all other cases, the calculated luminosity front is above the experimental results at the early stage of the flow and lower for the late development of the flow. The explanation is that initially the flow has a spherical symmetry but heat conduction to the walls results in losses which are more significant when the initial volume of the plasma is small. For this case, the ratio of wall surface in contact with the plasma to the volume of plasma is high; thus, high losses and a resultant lower-than-predicted velocity. As the flow develops, the cylindrical geometry of the plasma jet starts to form and the energy is dissipated in a volume smaller than the hemisphere used in the model. Thus, higher-than-predicted velocities are measured.

The results of calculated and measured shock wave positions are shown in Fig. 5, for the case of 900 V. Every

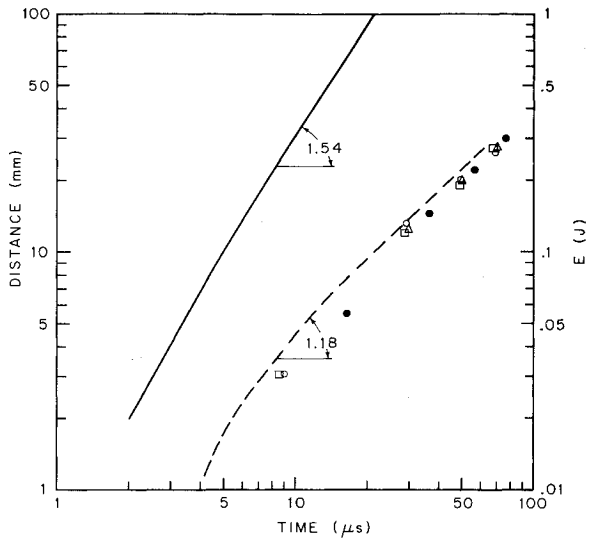

Fig. 5 Position of the shock front and the energy dissipated in the discharge vs time for 900 V. The dashed curve is the calculated position of the shock front and the various symbols are its measured position. Each symbol is the result of a different "shot." The solid line is the total energy dissipated, which was calculated from the measured dissipated power.

different symbol represents the result of a different "shot," and it is clear that the scattering is small. In Fig. 5, the energy obtained from the integration of input power is also shown. The curve is nearly linear (on this log-log plot) with a slope of 1.54 at 10 μs. As mentioned by Freeman, for a spherical, strong shock in which $E \propto t^{\beta}$, the self-similar treatment of the flow predicts a shock wave whose radius R is characterized by:

$$R = Kt^{n} \tag{6}$$

where K is a constant and

$$n = 2 + \beta/5 \tag{7}$$

For $\beta = 1.54$, $n = 0.71$. However, in our case, we obtained experimentally (see Fig. 5) $n = 1.18$ for a weak shock wave. Moreover, an accelerated strong shock wave in which $n > 1$ is predicted only for $\beta > 3$. We obtained an accelerated shock wave with $\beta = 1.54$. These results stress the fact that we are dealing with weak shocks and that one has to reply upon numerical calculation.

V. Conclusions

The measured positions of the luminosity front and shock front which result from time-dependent energy dissipation in a small cylindrical cavity have been reported. These measurements agree well with a numerical model proposed by Milinazzo et al.[13] This model assumes spherical symmetry, energy input which can be of any temporal form; the model is also applicable to weak shocks. The findings of this work give one confidence in applying the computational scheme to other geometries or even in using it to optimize energy input to practical igniters. For example, a series of numerical experiments (see Ref. 13 for details) in which the total energy dissipated as well as the functional form of the power was kept constant, but the time in which it was dissipated (t_0) was varied from 0.1-300 μs, the following results were obtained. As expected, the shock strength monotonically increased as t_0 decreased. However, the maximum depth of penetration of the luminous front occurred for $t_0 \approx 80$ μs. Thus, for an igniter where it is the depth of penetration of the luminous front which is important, the circuit can be designed to yield the appropriate, rather long, time constant.

Acknowledgments

The authors would like to acknowledge the assistance of R. Tront and helpful discussions with J. M. Dewey. The financial assistance of the National Research Council of Canada and the Universities of Alberta and Victoria are also gratefully acknowledged.

References

[1] Taylor, G. I., "The Formation of a Blast Wave by a Very Intense Explosion," *Proceedings of the Royal Society*, Ser. A, Vol. 201, March 1950, pp. 159-174.

[2] Sedov, L. I., "Unsteady Motions of Compressible Fluids," *Prikladnaya Mathematika i Mekhanika*, Vol. 9, 1945, pp. 293-311.

[3] Sakurai, A., "Blast Wave Theory," *Basic Developments in Fluid Dynamics*, M. Holt (Ed.), Academic Press, New York, 1965, pp. 309-375.

[4] Sedov, L. I., *Similarity and Dimensional Methods in Mechanics*, Academic Press, New York, 1959, Chap. 4.

[5] Freeman, R. A., "Variable Energy Blast Waves," *Journal of Physics, Series D*, Vol. 1, Dec. 1968, pp. 1697-1710.

[6] Pitkin, E. T., "Perturbation Solutions for Variable Energy Blast Waves," *Acta Astronautica*, Vol. 4, Nov.-Dec. 1977, pp. 1137-1158.

[7] Freeman, R. A. and Craggs, J. D., "Shock Waves from Spark Discharges," *Journal of Physics, Series D*, Vol. 2, March 1969, pp. 421-427.

[8] Dabora, E. K., "Variable Energy Blast Waves," *AIAA Journal*, Vol. 10, Oct. 1972, pp. 1384-1386.

[9] Hall, R. B., "Laser Production of Blast Waves in Low Pressure Gases," *Journal of Applied Physics*, Vol. 40, March 1969, pp. 1941-1945.

[10] Brode, H. L., "Numerical Solutions for Spherical Blast Waves," *Journal of Applied Physics*, Vol. 26, June 1955, pp. 766-775.

[11] Director, M. N. and Dabora, E. K., "Prediction of Variable-Energy Blast Waves," *AIAA Journal*, Vol. 15, Sept. 1977, pp. 1315-1321.

[12] Director, M. N. and Dabora, E. K., "An Experimental Investigation of Variable Energy Blast Waves," *Acta Astronautica*, Vol. 4, Feb. 1977, pp. 391-407.

[13] Milinazzo, F., Oved, Y., Clements, R. M., and Smy, P. R., "Blast Wave Computations Using the Flux-Corrected Transport Algorithm," *Journal of Physics, Series D*, to be published.

[14] Topham, D. R., Smy, P. R., and Clements, R. M., "An Investigation of a Coaxial Spark Igniter with Emphasis on its Practical Use," *Combustion and Flame*, Vol. 25, March 1975, pp. 187-195.

[15] Dale, J. D., Smy, P. R., and Clements, R. M., "The Effects of a Coaxial Spark Igniter on the Performance of and the Emissions from an Internal Combustion Engine," *Combustion and Flame*, Vol. 31, March 1978, pp. 173-185.

[16] Asik, J. R., Piatkowski, P., Foucher, M. J., and Rado, W. G., "Design of a Plasma Jet Ignition System for Automotive Application," SAE Paper 770355, Feb. 1977.

[17] Weinberg, F. J., Hom, K., Oppenheim, A. K., and Teichman, K., "Ignition by Plasma Jet," *Nature*, Vol. 272, March 1978, pp. 341-343.

[18] Ramsay, J. R. and Clements, R. M., "An Inexpensive Single-Scan Smear Camera," *Journal of Physics, Series E*, Vol. 10, Aug. 1977, pp. 780-782.

[19] Dewey, J. M. and Walker, D. K., "A Multiply Pulsed Double-Pass Schlieren System for Recording the Movement of Shocks and Particle Tracers Within a Shock Tube," *Journal of Applied Physics*, Vol. 46, Aug. 1975, pp. 3454-3458.

[20] Boris, J. P. and Book, D. L., "Flux-Corrected Transport I: SHASTA, a Fluid Transport Algorithm that Works," *Journal of Computational Physics*, Vol. 11, Jan. 1973, pp. 38-69.

[21] Book, D. L., Boris, J. P., and Hain, K., "Flux-Corrected Transport II: Generalizations of the Method," *Journal of Computational Physics*, Vol. 18, July 1975, pp. 248-283.

[22] Boris, J. P. and Book, D. L., "Solution of Continuity Equations by the Method of Flux-Corrected Transport," *Methods in Computational Physics*, Vol. 16, 1976, pp. 85-129.

[23] Boris, J. P. and Book, D. L., "Flux-Corrected Transport III: Minimal-Error Algorithms," *Journal of Computational Physics*, Vol. 20, April 1976, pp. 397-431.

[24] Boris, J. P., "Flux-Corrected Transport Modules for Solving Generalized Continuity Equations," Naval Research Laboratory, Memo. 3247, Washington, D.C., AD-A023 891/5G1, March 1976.